

RESEARCH

Open Access



Evaluation of closed-loop U-Tube deep borehole heat exchanger in the Basal Cambrian Sandstone formation, Alberta, Canada

Qinwan Chong, Jingyi Wang and Ian D. Gates*

*Correspondence:
ian.gates@ucalgary.ca

Department of Chemical
and Petroleum Engineering,
Schulich School of Engineering,
University of Calgary, Calgary, AB,
Canada

Abstract

Closed-loop deep borehole heat exchanger (DBHE) systems for producing heat from geothermal sources have the advantage that the heat transfer fluid is contained within the loop. In this study, for the first time, a U-configuration closed-loop DBHE was examined to evaluate the energy produced per unit energy invested from a 2330-m-deep geothermal reservoir in central Alberta, Canada. A detailed earth model where the system is modeled from the surface to the geothermal source is used in a numerical simulation model to understand the efficiency of the process. The results reveal that the fluid flow reaches its highest temperature in the ascending section of the U-loop rather than the bottom section which implies that the insulation on the working fluid should start in the ascending section of the U-loop. The results demonstrate that the closed-loop system can achieve ratios of the energy produced and energy invested of 7 GJ/GJ. Although this efficiency is promising, the absolute amount of heat energy harvested is limited by the loop's heat transfer area in the geothermal reservoir.

Keywords: Geothermal energy, Closed-loop well arrangement, Deep borehole heat exchanger, Energy return on energy invested, Energy efficiency

Introduction

With the focus on lowering the emissions intensities of energy with the eventual target of zero-emission energy, much attention has been focused on geothermal energy exploitation and production (Panwar et al. 2011; Gehringer and Victor 2012; IEA 2015; Nasruddin et al. 2016; Bertani 2016; Yildirim and Genc 2017). In geothermal systems, the produced temperature is the key parameter—the higher the working fluid temperature that can be realized from the reservoir, the greater the energy produced (Csányi et al. 2010). If sufficiently hot, say greater than about 90 °C, power can be produced (Lee 1996, 2001). In most geothermal designs, the working fluid injected into the hot reservoir strips heat from the rock and produces it to the surface for either generating power or providing heat (Balat et al. 2009; Molavi and McDaniel 2016). In these open-loop systems, the working fluid is typically the geothermal formation brine which can cause issues such as solids precipitation as the brine experiences different temperatures on its path from geothermal reservoir to surface and back (Izgec et al. 2005; Hebert et al. 2011;

Setiawan et al. 2019). Also, in some cases, disposal of the working fluid can be an issue (Robertson 1983; Sahar et al. 2010). Solid waste can also present challenges in open-loop systems (Vetter 1983).

An alternative to open-loop geothermal systems are closed-loop systems (Strang 2017) where the working fluid is circulated in a closed-loop through the geothermal reservoir from the surface (Carotenuto et al. 2001). In many applications, closed-loop systems are applied in shallow (<50 m) geothermal applications for household heating (Lund 2001). Ghoreishi-Madiseh et al. (2013) examined the use of shallow heat extraction from tailings ponds. Casasso and Sethi (2014) examined closed-loop geothermal heat pumps to determine key design parameters. Riahi et al. (2017) examined the use of closed-loop geothermal wells using super critical carbon dioxide as the working fluid. Recent work has been done on the use of closed-loop geothermal systems for deeper, greater than 2000 m deep, geothermal resources (Kohl et al. 2002). The main challenges faced by these systems are the drilling and completion technology to create the closed-loop system (Allahvirdizadeh 2020). The other key challenge faced by closed-loop systems is the amount of heat transfer that occurs across the loop from the geothermal reservoir (Cho et al. 2016). In these systems, heat is delivered only by thermal conduction from the formations directly surrounding the loop (Vany et al. 2020). Thus, the limited conductive heat transfer area is an issue.

For deep geothermal resources, the two main types of designs for closed-loop designs are the closed U-Tube and co-axial configurations (Pejic et al. 2005). The closed U-Tube is similar to that commonly applied in shallow geothermal systems (Song et al. 2017) with insulation placed to minimize heat losses (Zhang et al. 2019). The working fluid flows from the surface down one leg of the U to the target geothermal resource, then accumulates heat from the geothermal reservoir, and then flows back to the surface through another leg carrying the collected heat (Law et al. 2015). The co-axial well configuration has the wells in an annular arrangement: the outer annulus is used to carry the working fluid from the surface to the geothermal resource and a central flow pipe which conveys the working fluid back to the surface (Wood et al. 2012).

In a closed-loop system, the heat transfer area is the outer area of the flow loop wellbore itself (Alimonti et al. 2020). This means that the length of the loop or the number of closed laterals placed or both within the geothermal resource become key design parameters for the amount of heat produced. Another design parameter is the appropriate placement of insulation within the ascending part of the loop to minimize heat losses from the loop after the working fluid has achieved its maximum possible temperature. The circulating fluids in a closed-loop wellbore are completely isolated from underground hot rock and water existing in the reservoir. For closed-loop geothermal reservoir production, effective design of the loop placement, insulation length, and flow rate of the working fluid depends on an understanding of the anticipated temperature profile in the loop. Early studies mostly focus on achieving a targeted temperature profile at surface using traditional geothermal wellbores instead of closed-loop geothermal wellbore. Several models have been developed to predict temperature profiles (Sagar et al. 1991). In general, these models demonstrate the potential for energy recovery by using closed-loop well arrangements; in some cases, the maximum temperature occurs at the place at higher elevation than the well bottom (Kabir et al. 1996). In more complex

numerical models, Hecht-Méndez et al. (2013) demonstrated using numerical modeling that underground bore hole heat exchangers can be severely affected by groundwater flow. Radioti et al. (2016) investigated the impact of bedrock heterogeneity on the performance of a closed-loop geothermal system to identify correlations of the temperature profiles to the geological characteristics of the surrounding bedrock was identified. Wu et al. (2017) predicted heat extraction from a U-Tube closed-loop well in a geothermal reservoir using an approximate mathematical model; their results showed that heat extraction is affected by the injection rate, injection temperature and fluid viscosity. Song et al. (2018) studied heat production from a closed-loop geothermal system by analyzing temperature profile calculated through an unsteady state heat transfer model. The results indicated that heat production is mainly influenced by flow rate, inlet temperature, and horizontal heat exchanger section length. A critical flow rate was determined which yields the highest outlet temperature at surface. Sun et al. (2018) investigated the circulating process of CO₂ in a U-Tube closed-loop well. Gharibi et al. (2018) tested the feasibility of applying an abandoned oil well for geothermal energy development using a U-Tube heat exchanger in three-dimensional numerical model; the results proved that the repurposed well can be exploited to obtain heat for electricity generation and direct heating. Lyu et al. (2018) analyzed characteristics of a U-Tube heat exchanger in a geothermal well in Bazhou field, China and found that depth, porosity, permeability and heterogeneity of the formation influenced the system's performance. Toews et al. (2020) reported on the results of a closed-loop geothermal demonstration project (referred to as Eavor-Lite) near Sylvan Lake, Alberta, Canada. They showed energy production of about 0.44 MW (over a 30-day period) and the closeness of their simple radial conduction model and the field data reveal that the process is controlled by radial heat transfer to the well. Their heat transfer model did not account for heat losses through the well from the thermal reservoir to the surface and thus, the closeness of model and field data are surprising—Chong et al. (2021) revealed that heat losses in the production well can be significant. Data included in Beckers and Johnston (2022) reveal that the Eavor-Lite demonstration project realized an average produced temperature of about 52 °C (over about 15 months of operation) with an injected average temperature of 24 °C (a ~28 °C increase of temperature). Beckers and Johnston's model for application of the Eavor-Loop 2.0 in deeper and hotter formations suggest much higher production temperature although this has not yet been demonstrated in the field.

The optimal design and operating conditions of deep closed-loop geothermal systems, and in particular application to geothermal targets in Alberta, Canada, are not obvious and further work is needed for optimal design of these systems. Here, the results of a detailed numerical model are presented, for the first time, on a U-Tube closed-loop well configuration in the Basal Cambrian Sandstone Unit (BCSU) in central Alberta, Canada to yield optimal enthalpy delivery rates at surface. The objectives of the research presented here is to find the optimal circulation rate, the length of the heat exchanged in the geothermal target, placement of insulation, and temperature profile along the U-Tube loop.

Model description and equations

Geological model

The details of the geological model are described in Chong et al. (2021). In brief, the geological model is an earth model from the surface to the Basal Cambrian Sandstone unit (average depth 2330 m) in central Alberta, shown in Fig. 1. This geothermal reservoir has thickness of about 47 m with average temperature of 99.8 °C (Chong et al. 2021). From the surface, the overall vertical geothermal temperature gradient is equal to roughly 35.6 °C/km. The data used in the model are listed in Table 1. The geological model consists of 21 layers from the surface one more than the target geothermal reservoir. Each layer has its own rock and thermal properties (porosity, permeability, heat capacity, and thermal conductivity). The Basal Cambrian Sandstone unit is filled with water.

The geological model in this study is composed of 265,000 grid blocks in total with 50 grid blocks by 50 grid blocks in the horizontal directions and 106 grid block in the vertical direction. In both horizontal directions, the model has length of 1000 m with 20 m dimensions in each direction for each grid block. In the vertical direction, the total depth of the model is 2800 m with different grid block dimensions for each layer. The vertical grid block dimensions are smallest at the target geothermal formation. In the topmost surface formation, grid block height is the largest at 120.5 m, whereas in the target formation, the grid blocks heights are the smallest at 5.24 m. To examine whether the sensitivity of the results with respect to the dimensions of the grid blocks, a test was conducted with the grid blocks halved in all directions. The results (produced fluid temperature and temperature of the reservoir surrounding well) differed by less than 0.1%. Thus, the dimensions of the grid were deemed sufficiently refined for the study.

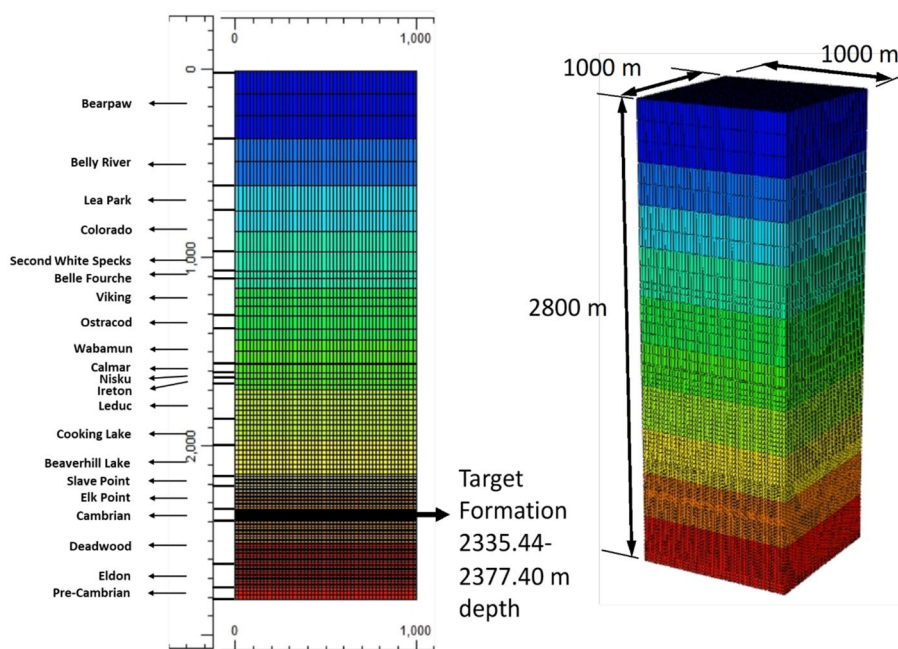


Fig. 1 Geological model

Table 1 Properties of the geological model (Chong et al. 2021)

Geological period	Formation	Rock type	Average depth (m)	Average thickness (m)	Average horizontal permeability (mD)	Average vertical permeability (mD)	Average porosity, fraction	Average compressibility (1/kPa)	Average heat capacity, J/m ³ °C	Average thermal conductivity, J/m day °C
Cretaceous	Bearpaw	Sandstone	303	361.5	39.12	7.66	0.2100	4.03×10^{-8}	2.50×10^6	2.68×10^5
Cretaceous	Belly River	Sandstone	361.5	245.6	452.96	232.31	0.2961	4.83×10^{-8}	2.50×10^6	2.68×10^5
Cretaceous	Lea Park	Sandstone	607.1	135.7	587.23	397.96	0.2377	4.27×10^{-8}	2.50×10^6	2.68×10^5
Cretaceous	Colorado	Sandstone	742.8	221	1998.0	21.30	0.1998	3.92×10^{-8}	2.50×10^6	2.68×10^5
Cretaceous	Second White Specks	Shale	963.8	99.0	0.47	0.03	0.0903	2.96×10^{-8}	2.50×10^6	1.81×10^5
Cretaceous	Belle Fourche	Shale	1062.8	38.1	129.05	53.09	0.1251	3.30×10^{-8}	2.50×10^6	1.81×10^5
Cretaceous	Viking	Sandstone	1100.9	201.2	28.77	9.55	0.1612	3.72×10^{-8}	2.50×10^6	2.68×10^5
Cretaceous	Ostracod	Sandstone	1302.1	65.5	1.88	0.50	0.1052	3.02×10^{-8}	2.50×10^6	2.68×10^5
Devonian	Wabamun	Dolomites	1367.6	179.9	11.45	6.13	0.0713	2.59×10^{-8}	2.50×10^6	4.06×10^5
Devonian	Calmar	Carbonate	1547.5	10.9	27.93	4.05	0.0603	2.42×10^{-8}	2.50×10^6	2.42×10^5
Devonian	Nisku	Sandstone	1558.4	43.6	19.17	5.07	0.0526	2.23×10^{-8}	2.50×10^6	2.68×10^5
Devonian	Ireton	Carbonate	1602	33.6	7.60	4.80	0.0435	1.99×10^{-8}	2.50×10^6	2.42×10^5
Devonian	Leduc	Carbonate	1635.6	188.9	516.44	201.49	0.0771	2.69×10^{-8}	2.50×10^6	2.42×10^5
Devonian	Cooking Lake	Carbonate	1824.5	133.8	314.72	367.08	0.0818	2.74×10^{-8}	2.50×10^6	2.42×10^5
Devonian	Beaverhill Lake	Carbonate	1958.3	180.5	9.58	4.36	0.0570	2.34×10^{-8}	2.50×10^6	2.42×10^5
Devonian	Slave Point	Siltstone	2138.8	33.2	0.23	0.03	0.0171	3.72×10^{-8}	2.50×10^6	2.33×10^5
Devonian	Elk Point	Siltstone	2172	158.2	1.13	0.2	0.0877	2.74×10^{-8}	2.50×10^6	2.33×10^5
Cambrian	Cambrian	Sandstone	2330.2	47.2	1.9	0.37	0.1484	3.63×10^{-8}	2.50×10^6	2.68×10^5
Cambrian	Deadwood	Sandstone	2377.4	237.2	1.2	0.21	0.0800	2.74×10^{-8}	2.50×10^6	2.68×10^5
Cambrian	Eldon	Sandstone	2614.6	123.7	1.0	0.17	0.0531	2.23×10^{-8}	2.50×10^6	2.68×10^5
	Pre-Cambrian	Crystal	2738.3	61.7	0.88	0.15	0.0250	1.53×10^{-8}	2.50×10^6	2.42×10^5

The geothermal target is the Basal Cambrian sandstone unit (highlighted in bold)

Governing equations in the geological domain

In the closed-loop system, there are two separate flow systems—the flow within the loop and the flow of water within the geothermal reservoir. These flows are coupled through conductive heat transfer through the wall of the flow loop. Here, both the fluid flow in the flow loop and the geothermal reservoir is modeled. In both systems, the material balance equation is (CMG 2019; Pruess and Narasimhan 1985):

$$\frac{\partial(V_v \rho)}{\partial t} = -\nabla \cdot (\rho \mathbf{u}) + q, \quad (1)$$

where V_v is void volume; ρ is mass density of water, t is time, \mathbf{u} is the velocity vector, and q represents net flow from external sources (for example adjacent water zones or the amount injected into a porous rock). In the porous geothermal reservoir rock, the velocity of brine is given by Darcy's law:

$$\mathbf{u} = -\frac{k}{\mu} (\nabla P - \rho g \nabla z), \quad (2)$$

where μ is the viscosity of the brine, k is the absolute permeability of the rock, P is the pressure, g is the acceleration due to gravity, and z is depth. In the porous reservoir rock, the conservation of energy is given by:

$$\frac{\partial}{\partial t} (V_s \rho U + V_s \rho_s C_s T) + \nabla \cdot (\rho \mathbf{u} H) - \nabla \cdot (k_{TH} \nabla T) = q_c - q_L, \quad (3)$$

where V_s is the volume of the rock, ρ_s is the density of the rock, C_s is the specific heat capacity of the rock, T is temperature, U and H are the specific internal energy and enthalpy of water, respectively, k_{TH} represents the effective thermal conductivity, q_c represents heat sources (for example the heat flux from the planet at the base of the domain), whereas q_L represents heat losses (for example to the atmosphere at the top of the domain).

Initial and boundary conditions of the geological domain

The surface temperature is constant at 16.85 °C and the temperature at the bottom of the domain (at 2797 m depth) is equal to 116.53 °C; we have assumed that the diffusion of the transient heat change due to the closed-loop system is slow compared to the heat flux provided from the planet below (this is a reasonable assumption given the temperature distribution results displayed below in Fig. 6). At the top and bottom boundaries, no flow is permitted. The pressure datum of the system is set to be equal to 30,000 kPa at depth 2350 m with hydrostatic pressure gradient prescribed. In all of the layers of rock which have non-zero porosity, the water saturation is taken to be 100%. The domain on its sides is connected to the rest of the planet and this is modeled by applying aquifers (large volume water grid blocks) at all layers at the boundaries of the model (CMG 2019). In each layer in the model, the pressure used in the aquifer model is equal to the initial hydrostatic pressure that existed in the model. However, since no overall horizontal pressure gradient is applied across the model

domain, there is no horizontal flow of water through the target geothermal reservoir (this could enhance heat transfer to the closed-loop well if it were present).

Governing equations for well model

In the work reported here, a U-Tube closed-loop well system based on existing designs (Schulz 2008; Wu et al. 2017; Sun et al. 2018) is applied for geothermal heat recovery, as shown in Fig. 2. There are three sections in the U-tube closed-loop: (1) a descending wellbore from the surface, (2) a horizontal wellbore to accumulate heat from the geothermal resource, and (3) an ascending wellbore conveying the heated working fluid to the surface. There is no fluid flow between the loop and the geothermal reservoir. This means that the reservoir geological properties, e.g., the porosity and permeability, can only affect the accumulation of heat in the working fluid due to the hydrological flow of brine moving past the well: beneficial in the descending section and the geothermal reservoir since the hotter formations provide heat to the working fluid or harmful in the ascending section where heat is lost from the working fluid to the surrounding formations. In the U-Tube, the first section descends to a depth of 2330 m. The second section

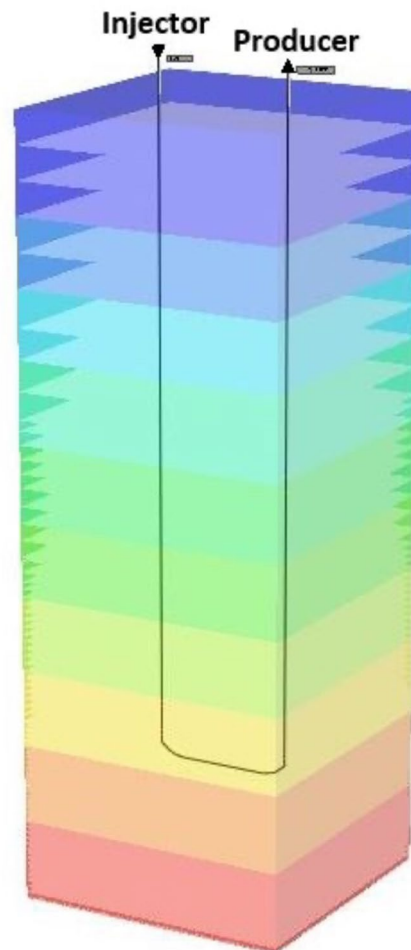


Fig. 2 U-Tube well configuration

is the horizontal part which is 400 m long. There are two kick-off intervals (transition from vertical to horizontal) at the ends of the horizontal interval—each is 50 m in horizontal extent and thus, the horizontal separation between the vertical intervals is 500 m.

The completion design for the vertical and horizontal intervals of the well is displayed in Fig. 3. The temperature of the underground increases with depth so as fluid flows down the descending section of the well, it starts to accumulate heat from the surrounding rock. As shown in Fig. 3a, the working fluid flows through an inner tubing string. In

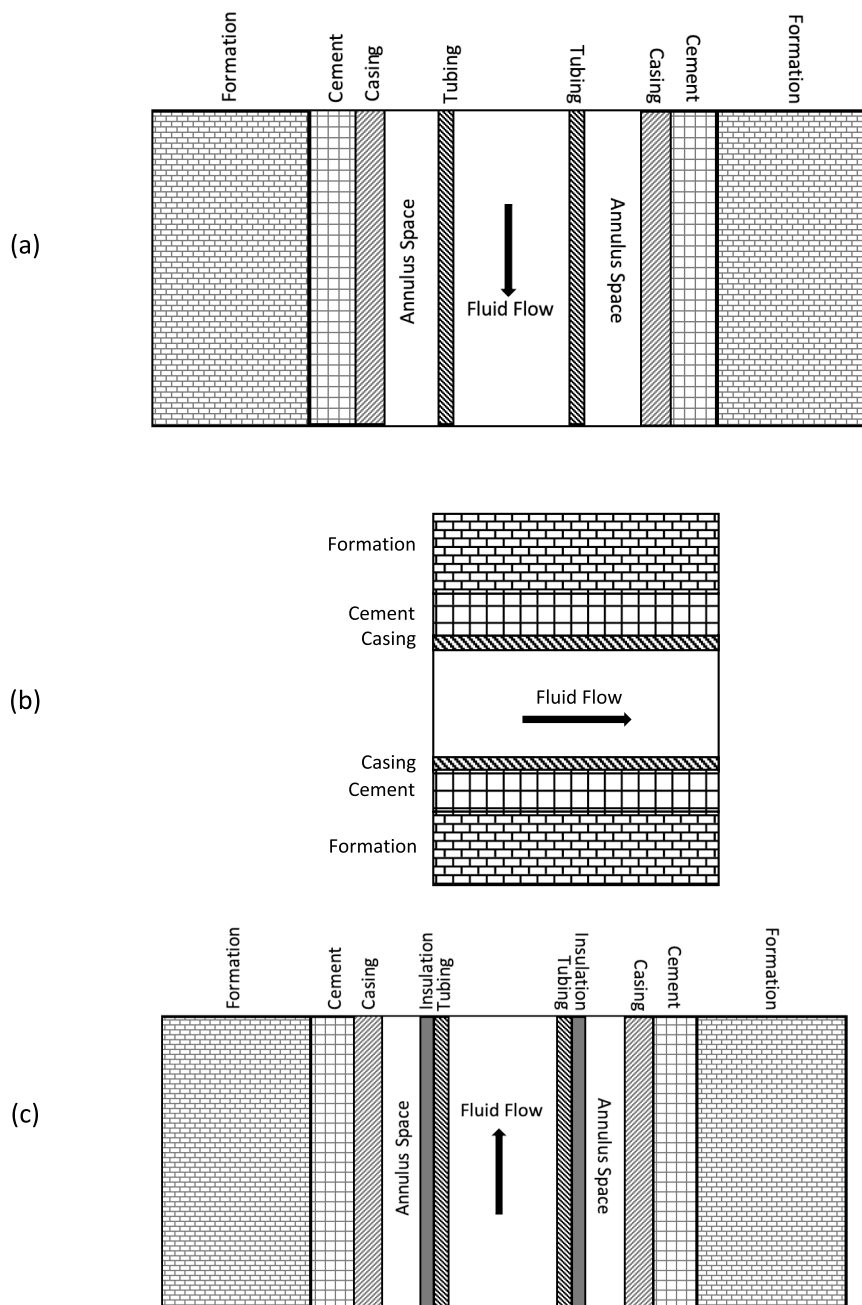


Fig. 3 Well completion design: **a** descending interval, **b** horizontal interval, and **c** ascending section

the descending section, there is no insulation and the annular space is filled with water. Heat transport from the surrounding rock goes through the cement and casing via conduction and then the annular space (convection and conduction), and then through the tubing string wall by conduction. After the fluid arrives at the bottom of the U-tube, it flows horizontally within the completion design shown in Fig. 3b. In this section, the working fluid flows through wellbore. After the fluid reaches the end of the horizontal section, in the ascending section, at the point where the working fluid starts to lose heat to the formation, as shown in Fig. 3c, the tubing string is insulated. In this section, the annular space is filled with gas to add further insulation to the tubing string.

In the annular space and tubing string, the pressure drop depends on viscous drag (friction), kinetic energy, and gravity; the method used here is based on Oballa et al. (1997). In this model, the pressure drop depends on the flow regime. The working fluid that flows through the closed tubing string is water and it remains as a single phase liquid at the conditions in the well. Under turbulent flow, the frictional pressure gradient is determined by:

$$\frac{\partial P}{\partial x} = \frac{2f\bar{u}^2}{D\rho}, \quad (4)$$

where f is the friction factor, determined from Colebrook's equation (Colebrook 1939), \bar{u} is the average fluid speed, D is the diameter of the tubing string, and ρ is the fluid density. In the annular space, the hydraulic diameter is given by:

$$D_h = 2 \left[r_a^2 + r_w^2 - \frac{r_a^2 - r_w^2}{\ln(r_a/r_w)} \right], \quad (5)$$

where r_a is the annulus radius and r_w is the wall radius. More details of the fluid flow in and between the tubing and annular spaces are described in CMG (2019). In each grid block containing the well, heat transfer occurs between the rock and the fluid within the tubing string according to a one-dimensional series radial heat transfer model where the heat transfer resistances are composed of the cement, casing, annulus space, insulation layer (if present), and tubing string wall. This means that the dimensions and thermal conductivities of each of these components must be specified and are listed in Table 2. For the tubing string, since flow occurs within it, the roughness must also be specified;

Table 2 Wellbore material properties (Gallup 2003; Engineering Toolbox 2003, 2005, 2008, 2018; Kaya and Hoşhan 2005; Thorbjörnsson 2017)

Object	Dimensions and other properties	Material	Thermal conductivity, W/m K
Tubing	Inner diameter 0.163 m Outer diameter 0.168 m Roughness 0.0001	Carbon steel	44.96
Insulation	Outer diameter 0.173 m	Calcium silicate	0.03
Casing	Outer diameter 0.23 m	Carbon steel	44.96
Annulus	Outer diameter 0.245 m	Water	0.66
Cement	Outer diameter 0.3 m	Cement	0.35

here, it is set equal to 0.0001. For heat transfer at the tubing string wall to the working fluid within, the heat transfer coefficient determined according to the method described by Fontanilla and Aziz (1982).

Numerical model

The reservoir simulation model uses the same grid block discretization as was used in the geological model. Tests were done to evaluate the impact of grid on the results. It was found that doubling the grid in each direction changed the results by less than 0.1% and thus, the grid block discretization shown in Fig. 4 was used for all cases (cases described below). In this study, the thermal reservoir simulation package CMG STARS™ (CMG 2019) is used to solve the governing equations as listed above. STARS™ is a commercial thermal reservoir simulator that uses the finite volume method together with Newton's method to solve the non-linear system of equations, Eqs. 1 to 4 above, for both flow and heat transfer in both the reservoir as well as the wells at each time step with Euler's method for time integration (CMG 2019). More details of the numerical approach is described in CMG (2019).

The trajectory of the well is shown in Fig. 2. The well is discretized from the surface to the target formation and back to the surface with each section of the well having a

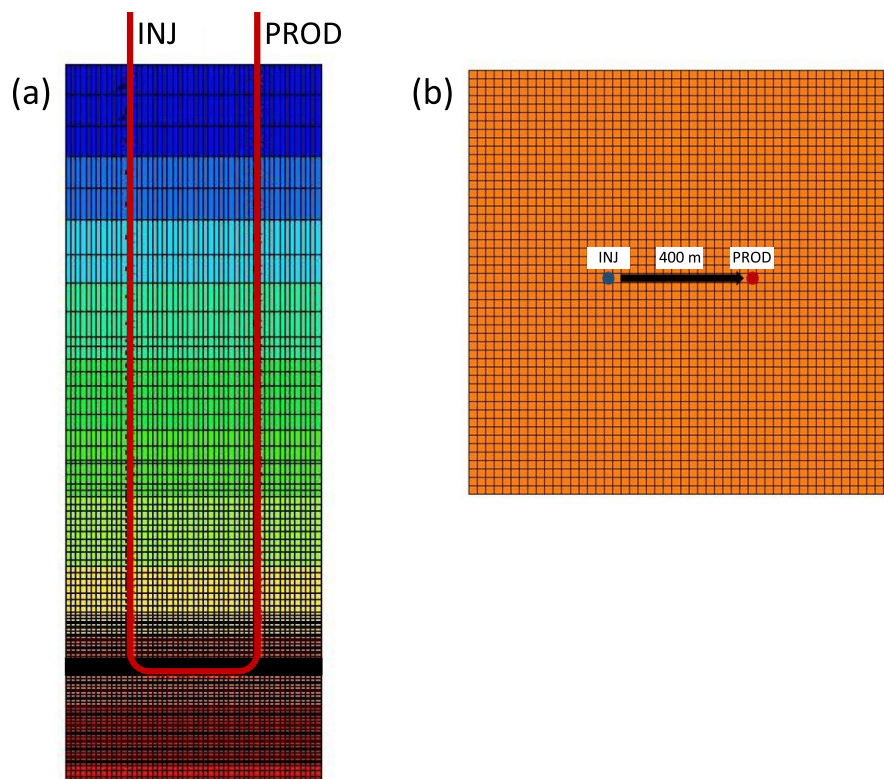


Fig. 4 Discretization of domain into grid blocks. In the vertical direction, shown in **a**, there are a total of 106 grid blocks with dimensions ranging from 5.24 to 120.5 m (finest grid blocks are in the geothermal reservoir). In the horizontal directions, shown in **b**, there are 50 × 50 grid blocks. INJ refers to the injection point of the well and PROD refers to the production point of the well

discretized length equal to the dimension of the grid block through which it is traversing in the vertical section, it is equal to the vertical dimension of the grid block and in the horizontal direction, it is equal to the horizontal dimension of the grid block. The CMG Flexwell (CMG 2019) model is used to model the well flow and enthalpy transfer. The tolerance on the linear solver is set equal to 10^{-6} . The models developed in this work were run on a 2.3 GHz workstation taking roughly 2 h per case using 2 cores in parallel solver mode.

U-Tube well operating conditions

The geothermal operation is run for 30 years (all year round). The working fluid is chosen as pure water. We examine five flow rate cases (100, 200, 300, and 400 m³/day) with and without insulation along the ascending section of the U-tube. The cases are listed in Table 3.

Results and discussion

Temperature profile

Figure 5 shows the temperature profile of all flow rate cases with and without insulation (when present, insulation only placed in the ascending section) versus the overall flow path versus time. The results show that as the flow rate is raised, the temperature realized by the working fluid before it enters the horizontal section is lower: after 1 year of operation, at 100 m³/day, the temperature of the working fluid before entering the horizontal section is equal to about 85 °C, whereas for the 400 m³/day case, the temperature reaches about 54 °C. After about 10 years, the temperature profiles have reached a quasi-steady state profile where the withdrawn heat is roughly equal to the amount replenished from below. This is also observed in Fig. 6 where the temperature distributions remain nearly unchanged after about Year 15. After 10 years, at 100 m³/day, the temperature of the working fluid before entering the horizontal section is equal to about 68 °C, whereas for the 400 m³/day case, the temperature reaches about 37 °C. In the 400-m horizontal section, after 10 years of operation, at 100 m³/day the temperature rises to 80 °C, whereas at 400 m³/day it increases to 53 °C. The temperature profiles reveal that in the no insulation case, at 100 m³/day, the highest temperature achieved by the working fluid is about 500 m beyond the end of the 400-m horizontal section in the ascending interval and when the fluid reaches the

Table 3 Summary of cases

Flow rate (m ³ /day)	Case
100	No insulation
	With insulation
200	No insulation
	With insulation
300	No insulation
	With insulation
400	No insulation
	With insulation

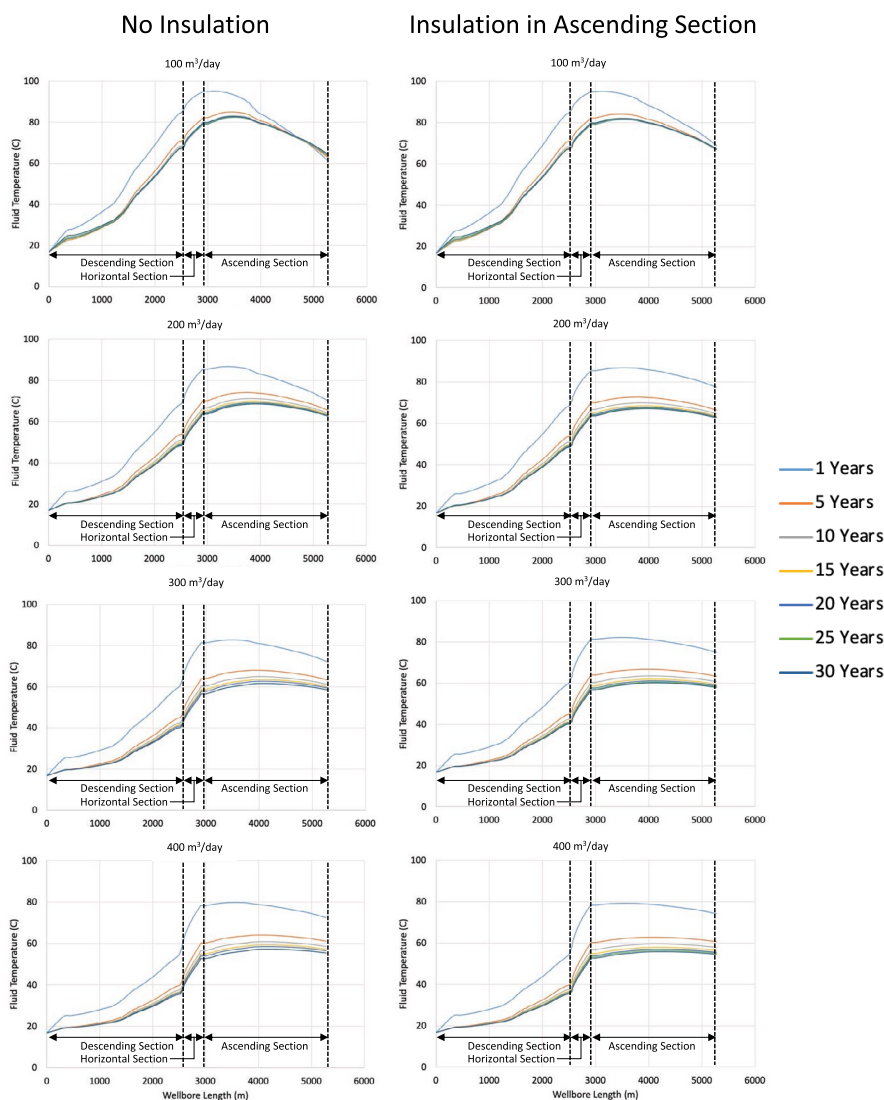


Fig. 5 Fluid temperature profiles versus path length versus flow rate and time in the case of no insulation

surface, the temperature drops to about 64 °C (for all time). At the higher flow rates, the maximum temperature achieved is generally between 500 and 700 m above the end of the horizontal section. The higher the flow rate, the lower is the heat losses in the ascending section. At 400 m³/day, after 10 years of operation, the temperature of the fluid at surface is equal to about 56 °C. The highest achieved temperature at the surface after 10 years of operations is at a flow rate of 200 m³/day at about 63 °C. As expected, when the insulation is present, the temperature of the produced fluid at surface is higher than that of the no insulation case. This is more pronounced at the lower flow rate: at Year 1, at 100 m³/day, the insulation in the ascending section maintains the temperature about 8 °C higher than that of the no insulation case; at 400 m³/day, the temperature difference is about 2 °C. Beyond Year 1, the temperature differences drop to below 2 °C for all flow rates. These results indicate that insulation may not be that beneficial given the flow rates considered here.

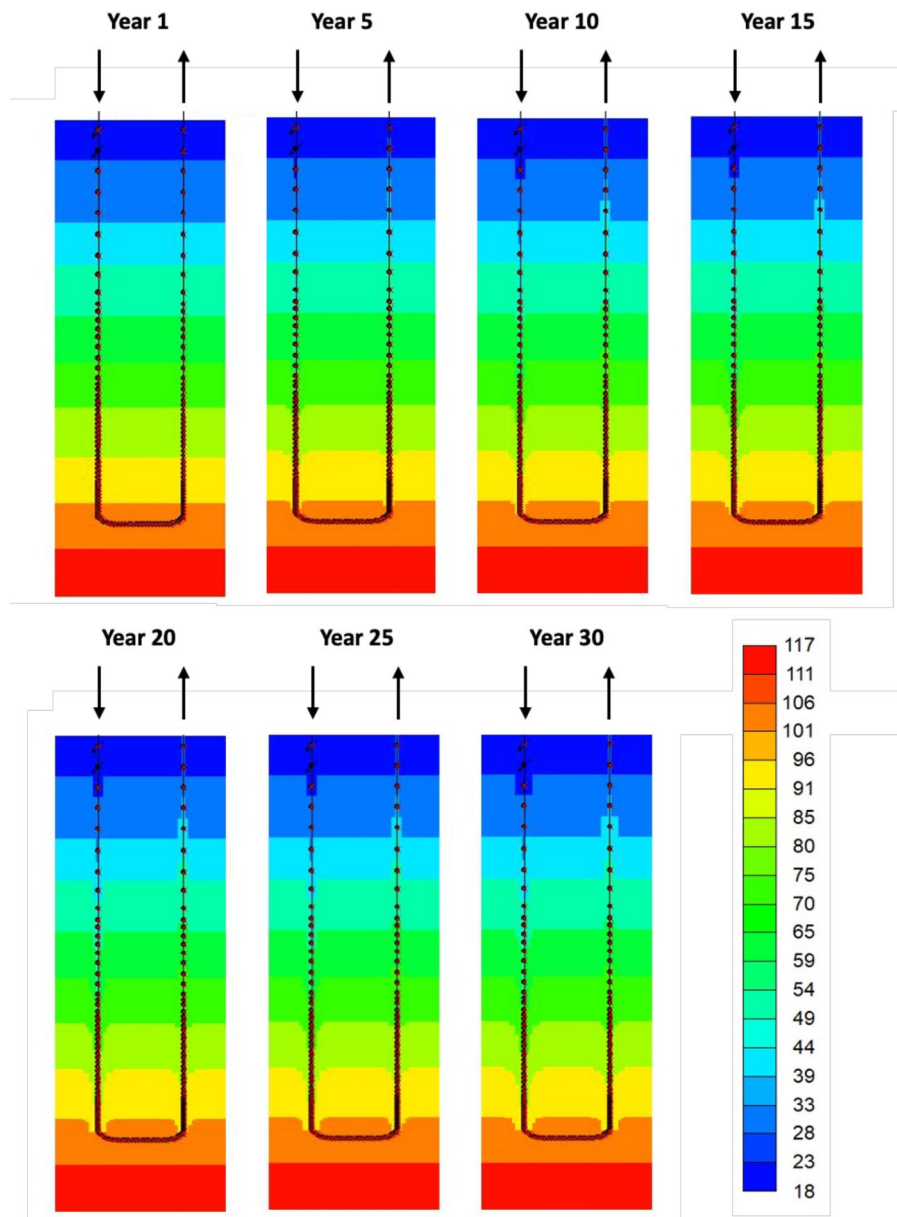


Fig. 6 Example of temperature distribution in the plane of the U-Tube well at flow rate of $400 \text{ m}^3/\text{day}$

Figure 6 displays the temperature distributions of the formations in the plane of the U-Tube loop versus time. The results show that the temperature of the formations in the near well region drops as the $16.85 \text{ }^\circ\text{C}$ water is injected downhole. The heat flux from below is sufficient to keep the temperature relatively constant in the geothermal reservoir. The temperature reduction observed in the near well region for the ascending section is due to the fluid being cooler than the formation there. However, higher up, about 700 m depth, the working fluid temperature is higher than that of the surrounding formation and the formation is heated by the working fluid. The distributions for the other flow rates are similar to that shown in Fig. 6.

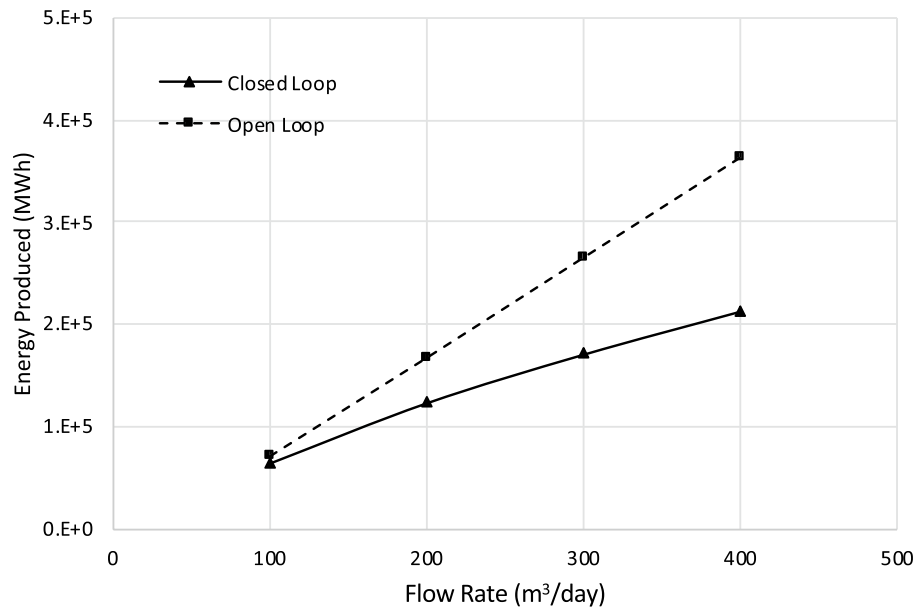


Fig. 7 Energy produced in closed and open-loop configurations (open-loop results from Chong et al. 2021)

Energy produced

Figure 7 compares the produced energy versus flow rate for the closed-loop configuration and a two-well open-loop configuration (with 500-m horizontal separation between the vertical wells) as reported in Chong et al. (2021) for flow through the Basal Cambrian Sandstone unit (same unit as used here for closed-loop system). In both cases, the greater the flow rate through the system, the higher is the produced energy. The absolute produced energy from the open-loop configuration is greater than that of the closed-loop case. This is because the available heat transfer area for the open-loop configuration where the working fluid flows through the geothermal reservoir rock is significantly larger than that of the closed-loop system.

Energy efficiency

Energy efficiency is indicated by the ratio of the energy produced from the geothermal resource at surface and the energy invested to move the working fluid through the loop, denoted as the EPEI (energy produced to energy invested) ratio; it is the same as the Coefficient of Performance, COP (Ghoreishi-Madiseh 2013; Cho et al. 2016; Zheng 2017):

$$\text{EPEI} = \frac{\text{Enthalpy produced from reservoir at surface}}{\text{Energy invested (e.g., pump energy)}}. \quad (6)$$

The energy invested is equal to the pump energy required for moving the fluid from the surface through the flow loop and back to the surface. Here, the pump efficiency is taken to be 75%.

Figure 8 displays the effect of working fluid flow rate on the EPEI for the closed-loop system as well as the equivalent open-loop system as described in Chong et al.

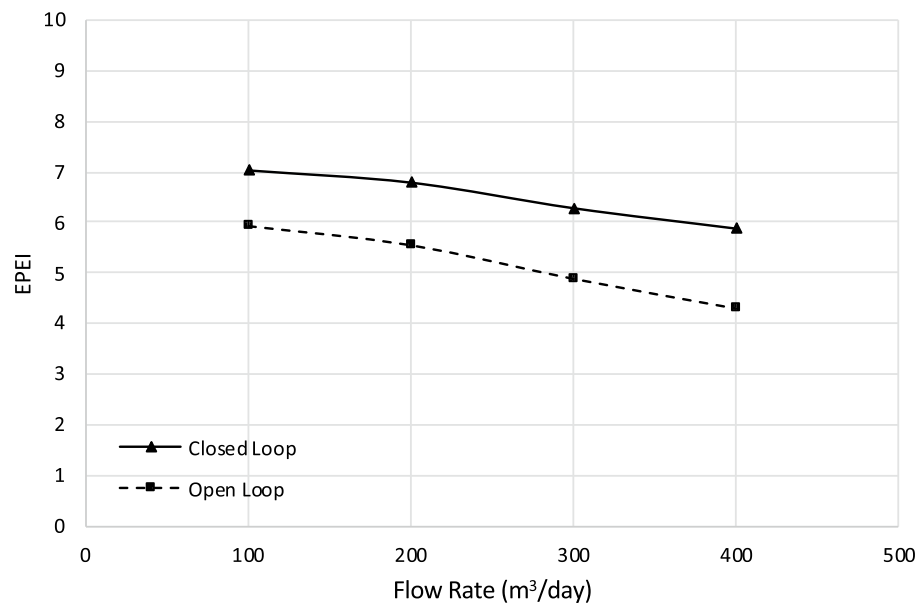


Fig. 8 Energy produced to energy invested ratio (EPEI) versus working fluid flow rate for the closed and open-loop geothermal systems (open-loop results from Chong et al. 2021)

(2021). The results show that for the closed-loop configuration, the highest EPEI ratio is equal to about 7 GJ/GJ when the flow rate is 100 m³/day whereas the lowest EPEI ratio reaches to about 5.8 GJ/GJ when the flow rate is 400 m³/day. The faster the flow of the circulating fluid, the lower the residence time of the fluid within the geothermal reservoir and thus, the lower the amount of recovered heat at surface—this implies a lower EPEI ratio. For the open-loop system, the EPEI is significantly lower than that of the closed-loop results with the highest result equal to 5.9 GJ/GJ at 100 m³/day and 4.3 GJ/GJ at 400 m³/day. The EPEI ratio also decreases faster in the open-loop system as the flow rate is raised. The reason for the lower EPEI ratio of the open-loop system is due to the additional pressure drop required to move the working fluid through the geothermal reservoir rock—this greater energy investment requirement causes the lower EPEI ratio for the open-loop system. In the closed-loop system, the amount of energy required to circulate the working fluid is far lower than that of the open-loop system. In a system with sufficiently high permeability of the geothermal reservoir, it could be the case that the resistance to flow in the reservoir is relatively low and thus the pump energy required is relatively low leading to an improved EPEI for the open-loop system. However, in the system we have examined here, given its permeability, the amount of invested energy to circulate the working fluid through the reservoir is high (Chong et al. 2021).

A lower limit for the EPEI has been defined by Hall et al. (2009) and is suggested to be equal to 3 GJ/GJ to be useful and beneficial to society. The results in Fig. 8 show that for both the open and closed-loop configurations that the EPEI exceeds 3.

Effect of horizontal section length in closed-loop system

Given the temperature profiles displayed in Fig. 5, the results suggest that the length of the horizontal section in the closed-loop system could be extended to improve the

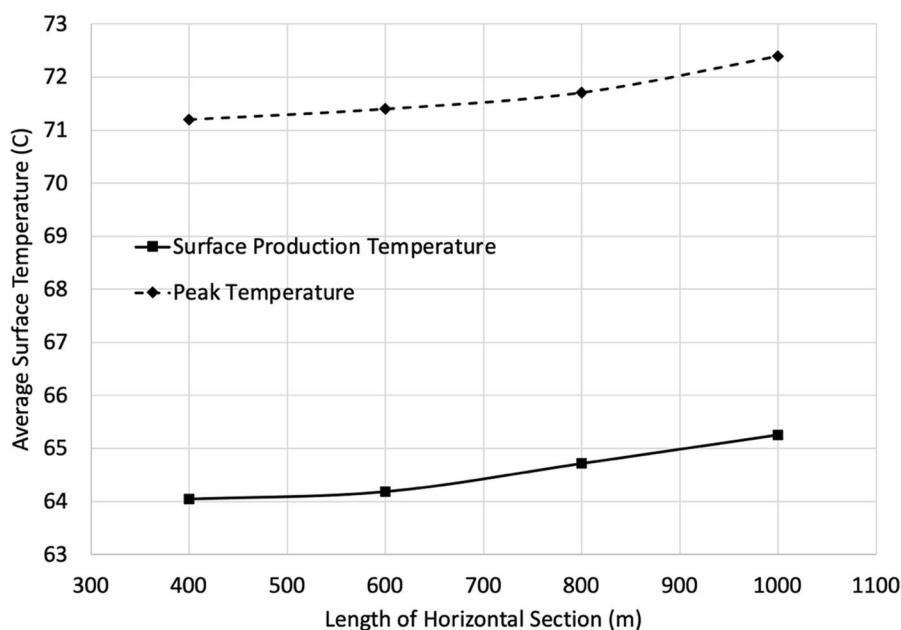


Fig. 9 Effect of length of horizontal section on the peak temperature and produced fluid temperature (temperature values are the average of the last 20 years for case of 200 m³/day working fluid flow rate)

amount of heat recovered from the reservoir. To test the effect of horizontal section length, the model (no insulation) was tested with horizontal lengths of 600, 800, and 1000 m at a flow rate of 200 m³/day. Figure 9 shows the rise of the averaged peak temperature achieved by the working fluid along the length of the U-tube loop and the surface produced average temperature (averages taken over the last 20 years of the operation) versus the length of the horizontal section. The results show that the temperature rise is relatively small (an increase of about 1.2 °C) even when the horizontal section is more than doubled to 1000 m. These results suggest that there is a benefit for extending the horizontal section length for this reservoir but that the rise of the surface produced temperature is of order of a few degrees. One reason for this small rise of temperature is because of the heat loss that occurs in the ascending section. As shown in Fig. 5, the peak temperature is reached in the ascending section. The hotter the fluid that is realized from the horizontal section, the greater the heat losses (the temperature difference is higher). This means that the combination of longer horizontal length with greater heat loss results in a relatively small temperature rise when the horizontal section is extended, as shown in the results in Fig. 9.

Figure 10 displays the relationship between the energy produced and the length of the horizontal section at a fluid flow rate of 200 m³/day for the closed-loop system. The results show that as the length of the well is increased from 400 to 1000 m, the amount of energy produced rises by about 6%. This increase of the energy suggest that the longer the well length, the greater is the energy harvested from the geothermal resource.

Figure 11 displays the effect of the length of the horizontal well section on the EPEI ratio at a flow rate of 200 m³/day for the closed-loop system. The results show that the EPEI ratio is lowest when the horizontal length is equal to 400 m. at longer horizontal lengths, the working fluid has a greater residence time in the geothermal reservoir to

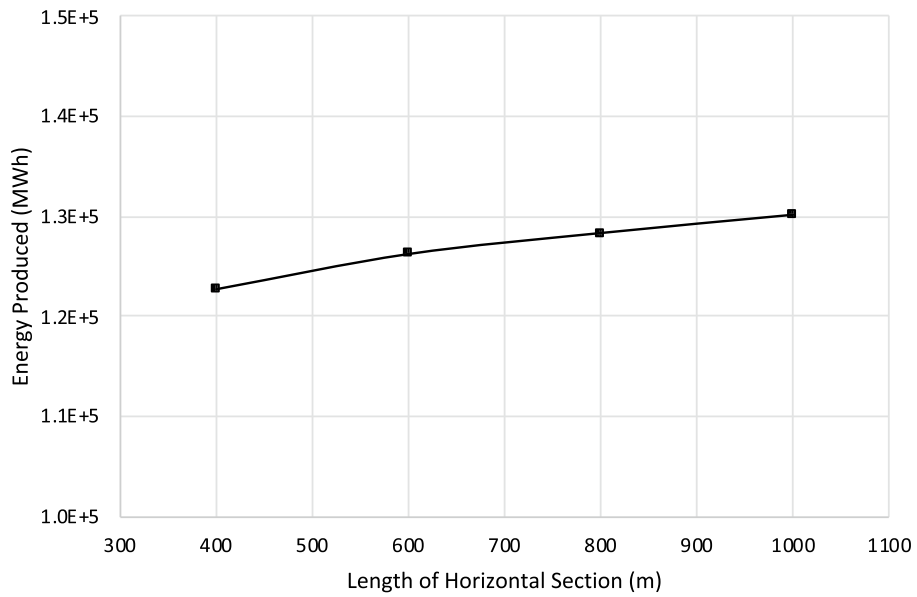


Fig. 10 Energy produced versus the length of the horizontal section for the closed-loop system at 200 m³/day fluid flow rate

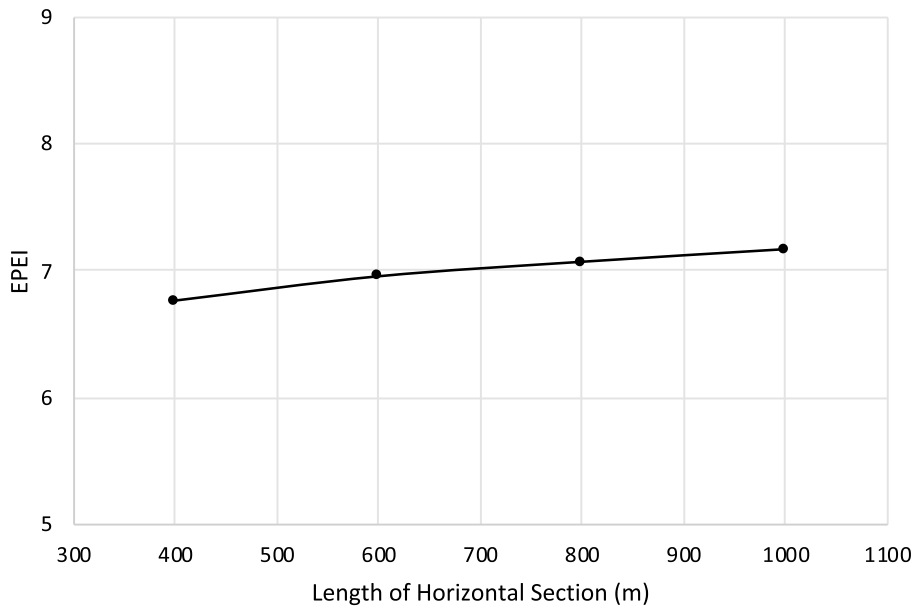


Fig. 11 EPEI versus the length of the horizontal section for the closed-loop system at 200 m³/day fluid flow rate

accumulate heat and thus, the EPEI ratio increases as a result. This result demonstrates that with respect to the EPEI ratio, the increased residence time created by the longer horizontal interval benefits the system over that of the additional working fluid pressure drop associated with the longer horizontal section.

The results illustrate that longer residence time within the horizontal well raises the EPEI. Longer residence time can be achieved by either lowering the circulation fluid flow

rate or longer horizontal well length or both. For applications in Alberta, and in particular, the Basal Cambrian Sandstone geothermal reservoir, the results demonstrate that the U-Tube system does not provide sufficiently hot fluid, with temperatures typically less than 70 °C, for production of electricity. This suggests that closed-loop technology for application in geothermal reservoirs such as the Basal Cambrian Sandstone unit will only have applications for district heating which might limit its energy and economic benefits to end-users local to the geothermal operation. The results uncover that there are risks for the application of closed-loop systems in geothermal reservoirs with properties similar to the one studied here or shallower reservoirs (where the temperature of the geothermal source would be lower than that of the system studied here and the realized surface temperature would be lower). Thus, a full economic analysis is required and consideration of closed-loop systems, if for electricity production, should be considered in deeper, more hot systems. This will imply greater cost for the wells and operating costs associated with circulating fluids through the loop. One option that could be used for lowering the invested energy in the process might be to use a thermosiphon for movement of a hot, vaporized working fluid to the surface.

Conclusions

For the first time, a closed-loop U-tube geothermal underground borehole heat exchanger has been examined the Basal Cambrian Sandstone geothermal resource at depth of 2330 m in Alberta, Canada. The analysis was conducted using a thermal reservoir simulator that solved both the flow and heat transfer equations in the reservoir rock as well as the loop well. The results demonstrate that the closed-loop system can yield energy produced to energy invested around 7 GJ/GJ for the working fluid flow rates and system geometry considered here. A comparison to open-loop system results for the same geothermal resource indicate that the closed-loop system is more energetically effective than that of the open-loop system, although the absolute energy recovered from the resource using the closed-loop system is smaller than that of the equivalent open-loop system. This suggests that the benefits of a U-Tube closed-loop system for low-grade geothermal resources, as is the case for the Basal Cambrian Sandstone geothermal resource, can be limited and a detailed analysis of the economics of the process should be examined. The findings show that insulation in the ascending section provides limited benefit with respect to the produced surface temperature especially at low flow rate—at high flow rate, the heat losses are even smaller. The results also suggested that produced surface temperature of the working fluid does not strongly depend on the length of the horizontal section in the U-Tube due to heat losses in the vertical section of the well system. Therefore, the use of U-Tube closed-loop systems for geothermal energy production should be considered for Albertan geothermal resources. However, the surface temperatures tend to range from 60 to 70 °C depending on the flow rate and insulation. Thus, the heat recovered would be best used for district heating.

Acknowledgements

The authors acknowledge support and guidance from Sinopec PEPRIS geothermal group and funding support from the University of Calgary's Canada First Research Excellence Fund program, the Global Research Initiative in Sustainable Low Carbon Unconventional Resources as well as the University of Calgary's Beijing Research Site.

Author contributions

QC, JW, IDG: conceptualization; QC: data curation; QC, JW: formal analysis; IDG: funding acquisition; QC, JW, IDG: investigation; QC, JW, IDG: methodology; IDG: project administration; IDG: resources; JW, IDG: software; IDG: supervision;

QC, JW: validation; QC, JW: visualization; QC, JW, IDG: roles/writing—original draft; IDG: writing—review and editing. All authors read and approved the final manuscript.

Funding

The authors acknowledge funding support from the University of Calgary's Canada First Research Excellence Fund program, the Global Research Initiative in Sustainable Low Carbon Unconventional Resources as well as the University of Calgary's Beijing Research Site.

Availability of data and materials

Models are available on request from corresponding author.

Declarations

Competing interests

The authors declare that they have no known competing financial interests or personal relationships that could have appeared to influence the work reported in this paper.

Received: 11 March 2022 Accepted: 12 September 2022

Published online: 01 October 2022

References

- Alimonti C, Conti P, Soldo E. Selecting the optimal use of the geothermal energy produced with a deep borehole heat exchanger: exergy performance. *Multidiscip Digit Publ Inst Proc.* 2020;58(1):20.
- Allahvirdizadeh P. A review on geothermal wells: well integrity issues. *J Clean Prod.* 2020;275: 124009.
- Balat M, Balat H, Faiz U. Utilization of geothermal energy for sustainable global development. *Energy Sources Part B.* 2009;4(3):295–309.
- Beckers KF, Johnson HE. Techno-economic performance of Eavor-Loop 2.0. In: *Proceedings 47th workshop on geothermal reservoir engineering*, Stanford, California, February 7–9; 2022.
- Bertani R. Geothermal power generation in the world 2010–2014 update report. *Geothermics.* 2016;60:31–43.
- Carotenuto A, Casarosa C, Vanoli L. Optimizing the position of the tube casing slotted section for geothermal wells with a downhole heat exchanger. *Geothermics.* 2001;30(1):133–57.
- Casasso A, Sethi R. Efficiency of closed loop geothermal heat pumps: a sensitivity analysis. *Renew Energy.* 2014;62:737–46.
- Cho JH, Nam Y, Kim HC. Performance and feasibility study of a standing column well (SCW) system using a deep geothermal well. *Energies.* 2016;9(2):1–13.
- Chong Q, Wang J, Gates I. Evaluation of energy extraction from a geothermal resource in central Alberta, Canada using different well configurations. *Geothermics.* 2021;96: 102222.
- Colebrook CR. Turbulent flow in pipes with particular reference to the transition region between smooth and rough pipe laws. *J Inst Civ Eng.* 1939;11:133.
- Computer Modelling Group Ltd. STARS™ user guide: advanced processes & thermal reservoir simulator version; 2019.
- Csányi L, Krištof V, Kušnir S, Katin M, Marci M. Geothermal energy. In: Paper presented at intensive programme “renewable energy sources”, Železná Ruda-Špičák, University of West Bohemia, Czech Republic, May; 2010.
- Engineering ToolBox. Thermal conductivity of some selected materials and gases. 2003. https://www.engineeringtoolbox.com/thermal-conductivity-d_429.html. Accessed 15 May 2019.
- Engineering ToolBox. Thermal conductivity of metals, metallic elements and alloys. 2005. https://www.engineeringtoolbox.com/thermal-conductivity-metals-d_858.html. Accessed 15 May 2019.
- Engineering ToolBox. Calcium silicate insulation. 2008. https://www.engineeringtoolbox.com/calcium-silicate-insulation-k-values-d_1171.html. Accessed 15 May 2019.
- Engineering ToolBox. Water—thermal conductivity. 2018. https://www.engineeringtoolbox.com/water-liquid-gas-thermal-conductivity-temperature-pressure-d_2012.html. Accessed 15 May 2019.
- Fontanilla JP, Aziz K. Prediction of bottom-hole conditions for wet steam injection wells. *J Can Pet Technol.* 1982. <https://doi.org/10.21118/82-02-04>.
- Gallup DL. Corrosion of piping under insulation in geothermal energy extraction processes. In: Paper presented at NACE—international corrosion conference, San Diego, California, USA, March 16–20; 2003.
- Gehring M, Victor L. *Geothermal handbook: planning and financing power generation.* Washington, DC: ESMAP; 2012.
- Gharibi S, Mortezaazadeh E, Hashemi Aghcheh Bodi SJ, Vatani A. Feasibility study of geothermal heat extraction from abandoned oil wells using a U-tube heat exchanger. *Energy.* 2018;153:554–67.
- Ghoreishi-Madiseh SA, Hassani FP, Mohammadian A, Radziszewski PH. A study into extraction of geothermal energy from tailings ponds. *Int J Min Reclam Environ.* 2013;27(4):257–74.
- Hall CAS, Balogh S, Murphy DJR. What is the minimum EROI that a sustainable society must have? *Energies.* 2009;2(1):25–47.
- Hebert R, Ledesert B, Genter A, Bartier D, Dezayes C. Mineral precipitation in geothermal reservoir: the study case of calcite in the Soultz-sous-Forets enhanced geothermal system. In: *Proceedings, thirty-sixth workshop on geothermal reservoir engineering*, Stanford University, Stanford, California, January; 2011.
- Hecht-Méndez J, De Paly M, Beck M, Bayer P. Optimization of energy extraction for vertical closed-loop geothermal systems considering groundwater flow. *Energy Convers Manag.* 2013;66:1–10.
- IEA. *Medium-term renewable energy market report.* Paris: OECD/IEA; 2015.
- Izgec O, Demiral B, Bertin H, Akin S. Calcite precipitation in low temperature geothermal systems: an experimental approach. In: *Proceedings thirtieth workshop on geothermal reservoir engineering*, (May 2014); 2005. p. 1–6.

- Kabir CS, Hasan AR, Kouba GE, Ameen MM. Determining circulating fluid temperature in drilling, workover, and well-control operations. *SPE Drill Complet.* 1996;11(2):74–8.
- Kaya T, Hoşhan P. Corrosion and material selection for geothermal systems. In: Paper presented at proceedings world geothermal congress 2005, Antalya, Turkey, April 24–29; 2005.
- Kohl T, Brenni R, Eugster W. System performance of a deep borehole heat exchanger. *Geothermics.* 2002;31(6):687–708.
- Law R, Bridgland D, Nicholson D, Chendorain M. Heat extraction from deep single wells. In: Thirty-ninth workshop on geothermal reservoir engineering, (April); 2015. p. 1–12.
- Lee KC. Classification of geothermal resources by exergy. *Geothermics.* 2001;30(4):431–42.
- Lee KC. Classification of geothermal resources—an engineering approach. In: Twenty-first workshop on geothermal reservoir engineering. 1996;1:85–92.
- Lund JW. Chapter 2.4: Design of closed-loop geothermal heat exchangers in the U.S. international summer school on direct application of geothermal energy, IGA; 2001. p. 1–13.
- Lyu Z, Song X, Li G, Shi Y, Mu Z. Numerical analysis of characteristics of a single U-tube downhole heat exchanger in a geothermal well. *Geothermics.* 2018;72:5–23.
- Molavi J, McDaniel J. A review of the benefits of geothermal heat pump systems in retail buildings. *Procedia Eng.* 2016;145:1135–43.
- Nasruddin N, Alhamid MI, Daud Y, et al. Potential of geothermal energy for electricity generation in Indonesia: a review. *Renew Sustain Energy Rev.* 2016;53:733–40.
- Oballa V, Coombe DA, Buchanan L. Aspects of discretized wellbore modelling couple to compositional/thermal simulation. *J Can Pet Technol.* 1997. <https://doi.org/10.2118/97-04-04>.
- Panwar NL, Kaushik SC, Kothari S. Role of renewable energy sources in environmental protection: a review. *Renew Sustain Energy Rev.* 2011;15(3):1513–24.
- Pejic D, Stojiljkovic D, Stojiljkovic S, Djurovic-Petrovic M, Mitic N. Geothermal heat exchanger with coaxial flow of fluids. *Hemijaska Industrija (Chem Ind).* 2005;59(9–10):275–8.
- Pruess K, Narasimhan TN. A practical method for modeling fluid and heat flow in fractured porous media. *Soc Pet Eng.* 1985;25(1):14–26.
- Radioti G, Delvoie S, Charlier R, Dumont G, Nguyen F. Heterogeneous bedrock investigation for a closed-loop geothermal system: a case study. *Geothermics.* 2016;62:79–92.
- Riahi A, Moncarz P, Kolbe W, et al. Innovative closed-loop geothermal well designs using water and super critical carbon dioxide as working fluids. In: Proceedings, forty-second workshop on geothermal reservoir engineering, Stanford University, Stanford, CA, USA, 13–15 February 2017; 2017.
- Robertson RC. Waste heat disposal from US geothermal power plants—an update. *Geothermics.* 1983;12(1):17–28.
- Sagar R, Doty DR, Schmidt Z. Predicting temperature profiles in a flowing well. *SPE Prod Eng.* 1991;6(4):441–8.
- Sahar S, Zarandi MM, Boulvar B. Wastewater disposal at the Nesjavellir geothermal power plant. In: Proceedings of the world geothermal congress 2010 Bali, Indonesia, April (13); 2010. p. 277–301.
- Schulz SU. Investigations on the improvement of the energy output of a closed loop geothermal system (CLGS). PhD thesis, Technical University of Berlin. 2008.
- Setiawan FA, Rahayuningsih E, Petrus HTBM, Nurpratama MI, Perdana I. Kinetics of silica precipitation in geothermal brine with seeds addition: minimizing silica scaling in a cold re-injection system. *Geotherm Energy.* 2019;7(1):1–16.
- Song X, Shi Y, Li G, Yang R, Xu Z, Zheng R, Wang G, Lyu Z. Heat extraction performance simulation for various configurations of a downhole heat exchanger geothermal system. *Energy.* 2017;141:1489–503.
- Song X, Shi Y, Li G, Shen Z, Hu X, Lyu Z, Zheng R, Wang G. Numerical analysis of the heat production performance of a closed loop geothermal system. *Renew Energy.* 2018;120:365–78.
- Strang KD. Innovative closed-loop underground pumped hydroelectricity geothermal storage system. *Int J Environ Stud.* 2017;74:363–85.
- Sun F, Yao Y, Li G, Li X. Geothermal energy development by circulating CO₂ in a U-shaped closed loop geothermal system. *Energy Convers Manag.* 2018;174:971–82.
- Thorbjornsson I. Candidate materials for couplings and casings. Zenodo. 2017. <https://doi.org/10.5281/ZENODO.1287569>.
- Toews M, Riddell D, Vany J, Schwarz B. Case study of a multilateral closed-loop geothermal system. In: Proceedings world geothermal congress, Reykjavik, Iceland, April 26–May 2; 2020.
- Vany J, Hirschmiller J, Toews M. Subsurface characterization methods for multilateral closed loop geothermal systems. Case study of field scale technology demonstration project in Alberta, Canada. *GRC Trans.* 2020;44(December):1360–1.
- Vetter OJ. Solid waste problems in geothermal operations. Society of Petroleum Engineers—SPE California regional meeting, CRM 1983; 1983. p. 767–74.
- Wood CJ, Liu H, Riffat SB. Comparative performance of “U-tube” and “coaxial” loop designs for use with a ground source heat pump. *Appl Therm Eng.* 2012;37:190–5.
- Wu B, Ma T, Feng G, Chen Z, Zhang X. An approximate solution for predicting the heat extraction and preventing heat loss from a closed-loop geothermal reservoir. *Geofluids.* 2017;2017:1–17.
- Yildirim N, Genc S. Energy and exergy analysis of a milk powder production system. *Energy Convers Manag.* 2017;149(1):698–705.
- Zhang Y, Yu C, Li G, Guo X, Wang G, Shi Y, Peng C, Tan Y. Performance analysis of a downhole coaxial heat exchanger geothermal system with various working fluids. *Appl Therm Eng.* 2019;163(January): 114317.
- Zheng H. Chapter 8: Absorption and adsorption solar desalination system. In: *Solar energy desalination technology*. Elsevier: Amsterdam; 2017. p. 623–70.

Publisher's Note

Springer Nature remains neutral with regard to jurisdictional claims in published maps and institutional affiliations.